The EMBO Journal Vol. 21 No. 16 pp. 4307–4316, 2002

Endothelium-specific platelet-derived growth factor-B ablation mimics diabetic retinopathy

Maria Enge, Mattias Bjarnegård, Holger Gerhardt, Erika Gustafsson[1], Mattias Kalén[2], Noomi Asker[2], Hans-Peter Hammes[3], Moshe Shani[4], Reinhardt Fässler[5] and Christer Betsholtz[6]

Department of Medical Biochemistry, Göteborg University, PO Box 440, SE 405 30 Göteborg, [1]Department of Experimental Pathology, Lund University, SE 221 85 Lund, [2]AngioGenetics AB, Medicinaregatan 7, SE 413 90 Göteborg, Sweden, [3]Vth Medical Clinic, Medical Faculty of the University of Heidelberg, D-68135 Mannheim, Germany, [4]Institute of Animal Science, The Volcani Center, Bet Dagan 50250, Israel and [5]Max Planck Institute for Biochemistry, Department of Molecular Medicine, Am Klopferspitz 18a, D-82152 Martinsried, Germany

[6]Corresponding author
e-mail: Christer.Betsholtz@medkem.gu.se

Loss of pericytes from the capillary wall is a hallmark of diabetic retinopathy, however, the pathogenic significance of this phenomenon is unclear. In previous mouse gene knockout models leading to pericyte deficiency, prenatal lethality has so far precluded analysis of postnatal consequences in the retina. We now report that endothelium-restricted ablation of platelet-derived growth factor-B generates viable mice with extensive inter- and intra-individual variation in the density of pericytes throughout the CNS. We found a strong inverse correlation between pericyte density and the formation of a range of retinal microvascular abnormalities strongly reminiscent of those seen in diabetic humans. Proliferative retinopathy invariably developed when pericyte density was <50% of normal. Our data suggest that a reduction of the pericyte density is sufficient to cause retinopathy in mice, implying that pericyte loss may also be a causal pathogenic event in human diabetic retinopathy.

Keywords: Cre-loxP system/diabetes/pericytes/platelet-derived growth factor/retinopathy

Introduction

All capillaries are partially covered by mural cells of the vascular smooth muscle cell (vSMC) lineage, referred to as pericytes. A number of murine gene knockout mutations interrupting signaling by platelet-derived growth factor (PDGF)-B/PDGF receptor-β (PDGFR-β), angiopoietin-1/Tie-2, TGF-β and EDG-1 lead to pericyte- and/or vSMC deficiency. These mutants are all lethal before birth due to cardiovascular dysfunction (Levéen *et al*., 1994; Soriano, 1994; Suri *et al*., 1996; Lindahl *et al*., 1997; Patan, 1998; Li *et al*., 1999; Yang *et al*., 1999; Liu *et al*., 2000; Oh *et al*., 2000). TGF-β signaling appears to be critical for early vSMC/pericyte formation, whereas PDGF-B/R-β and EDG-1 signaling seems to be involved in later proliferation and migration of these cells. Angiopoietin-1 targets primarily Tie-2 receptors on endothelial cells and its role in vSMC/pericyte formation might therefore be indirect.

The only disease strongly linked to pericyte deficiency is diabetic retinopathy. The pericyte density is higher in retinal than in other capillaries (Sims, 1986), probably reflecting a particularly important function at this location. Pericyte loss is the earliest morphological sign of retinal vascular abnormalities in diabetes (Cogan *et al*., 1961); however, whether it constitutes a causal event in, or a mere consequence of, the pathogenesis of diabetic retinopathy is unknown. Pericytes may produce survival signals for endothelial cells (Benjamin *et al*., 1998, 1999), and loss of pericytes may therefore provoke endothelial death and the formation of acellular (regressing) capillaries, which are typically increased in diabetic retinopathy. It has also been suggested that pericyte loss may cause local weakenings leading to outpouchings (microaneurysms) in the capillary wall (Cogan *et al*., 1961; Buzney *et al*., 1977). Lack of pericytes in PDGF-B- or PDGFR-β-deficient embryos leads to the formation of capillaries with highly variable diameter (Hellström *et al*., 2001). Since vessel wall tension is proportional to its radius at constant blood pressure (law of Laplace), focal dilations may rapidly expand to microaneurysms. Indeed, pericyte-deficient *PDGF-B* and *PDGFR*-β null mice develop numerous rupturing microaneurysms at late gestation, when blood pressure is increasing (Levéen *et al*., 1994; Soriano, 1994; Lindahl *et al*., 1997; Hellström *et al*., 1999). These vascular lesions are reminiscent of those seen in human diabetic microangiopathy, providing support for a causal role of pericyte loss in the pathogenesis of this disease. Moreover, the importance of the PDGF-B/PDGFR-β signaling pathway for pericyte recruitment in the retina was demonstrated recently in a mouse model in which the intracellular domain of PDGFR-β was exchanged for that of PDGFR-α (Klinghoffer *et al*., 2001). These mice develop severe vascular changes and retinopathy, most likely because of failure of proper pericyte recruitment. Data from diabetic rodents, however, conflict somewhat with the view that pericyte loss is a causal event in diabetic retinopathy. Such animals lose up to 50% of the retinal pericytes (Buscher *et al*., 1989; Engerman, 1989) and develop increased numbers of acellular capillaries, but microaneurysms are rare, and more importantly, progression into the severe proliferative type of retinopathy is never seen. Thus, only the earliest and mildest signs of human diabetic retinopathy are seen in diabetic rodents, in spite of significant pericyte loss.

Here, we have used the Cre-loxP system to target an inactivating mutation to the mouse *PDGF-B* gene selectively in endothelial cells. Such mutant mice survived postnatally and showed a high degree of inter- and

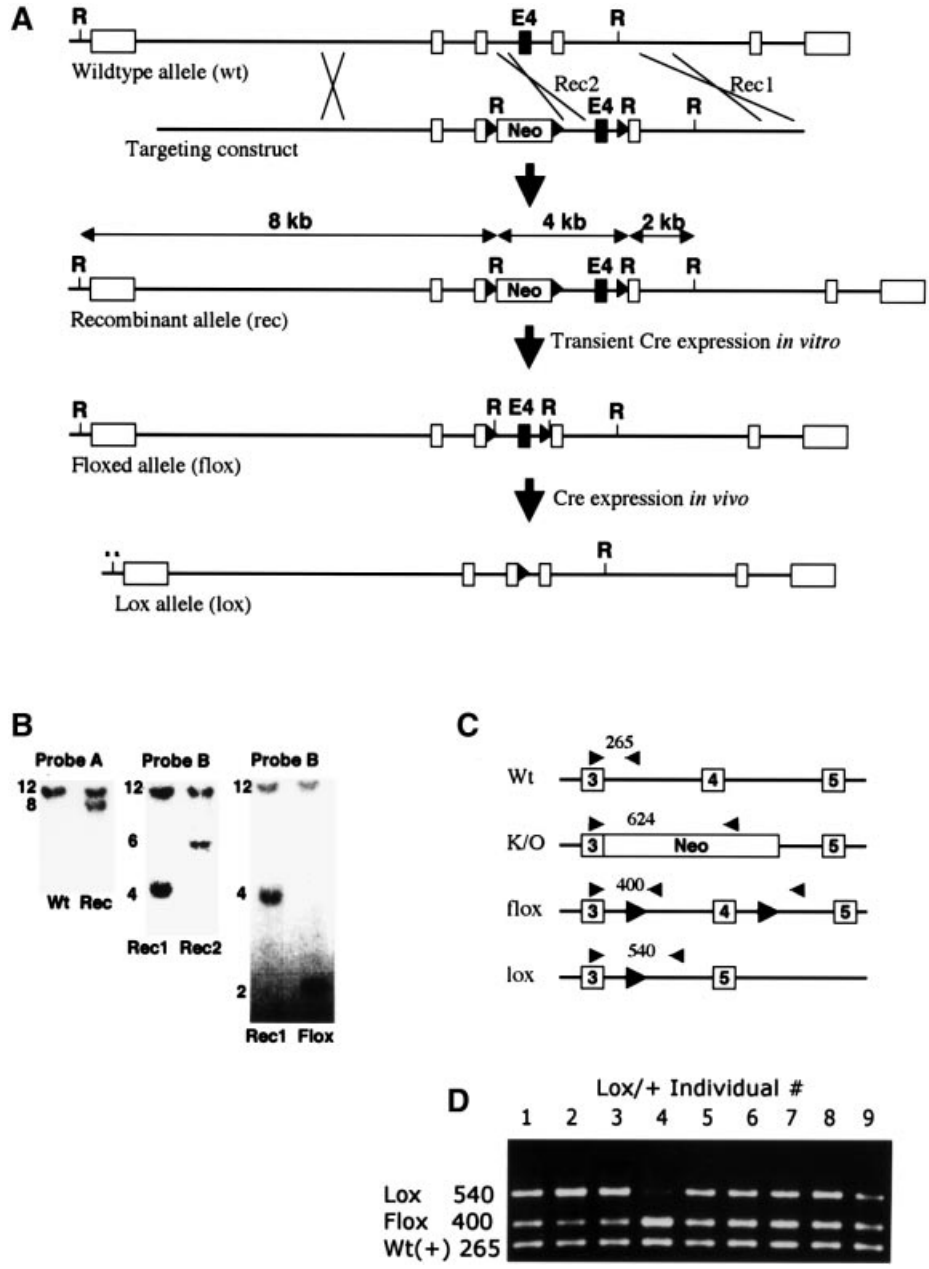

Fig. 1. Generation of mice with endothelium-restricted PDGF-B inactivation. (**A**) Partial maps of the wild-type, recombinant, flox and lox alleles and the targeting construct. Boxes indicate exons. E4, exon 4; Neo, PGK-neo cassette; R, *Eco*RI site. Black triangles denote loxP sites. (**B**) Southern blot analysis of genomic *Eco*RI digests showing examples of initial discrimination between wild-type and recombinant alleles (left), discrimination between recombination on either side of the 3′ loxP site (middle) and conversion from recombinant to flox allele (right). Probes used are indicated in (A). (**C**) Outline of PCR strategies used to discriminate between PDGF-B wild-type, flox, lox and knockout (K/O) alleles. (**D**) Genotyping of brain microvascular fragments. Lanes 1–9 represent fragment preparations from different lox/+ individuals. Note the inter-individual variation in flox–lox conversion. The intensity of the wild-type allele PCR fragment was similar in all individuals, serving as a control for the PCR.

intra-individual variation in the recruitment of pericytes to blood vessels in the CNS, including the retina. Hence, they were suitable for the analysis of the consequences of different extents of pericyte deficiency in the retina. We took advantage of the variation in pericyte recruitment to establish a strong correlation between the degree of pericyte reduction and the development of a spectrum of retinal vascular changes reminiscent of those observed in non-proliferative, as well as in proliferative, diabetic retinopathy.

Results

Generation of mice with endothelium-restricted deletion of PDGF-B

We placed loxP sites on each side of *PDGF-B* exon 4, thereby producing a *PDGF-B*^{flox} allele, and mice carrying this allele were generated (Figure 1 and Materials and methods). *PDGF-B*$^{flox/flox}$ and *PDGF-B*$^{flox/-}$ mice were normal, demonstrating functional activity of the *PDGF-B*^{flox} allele. We crossed mice expressing the Cre

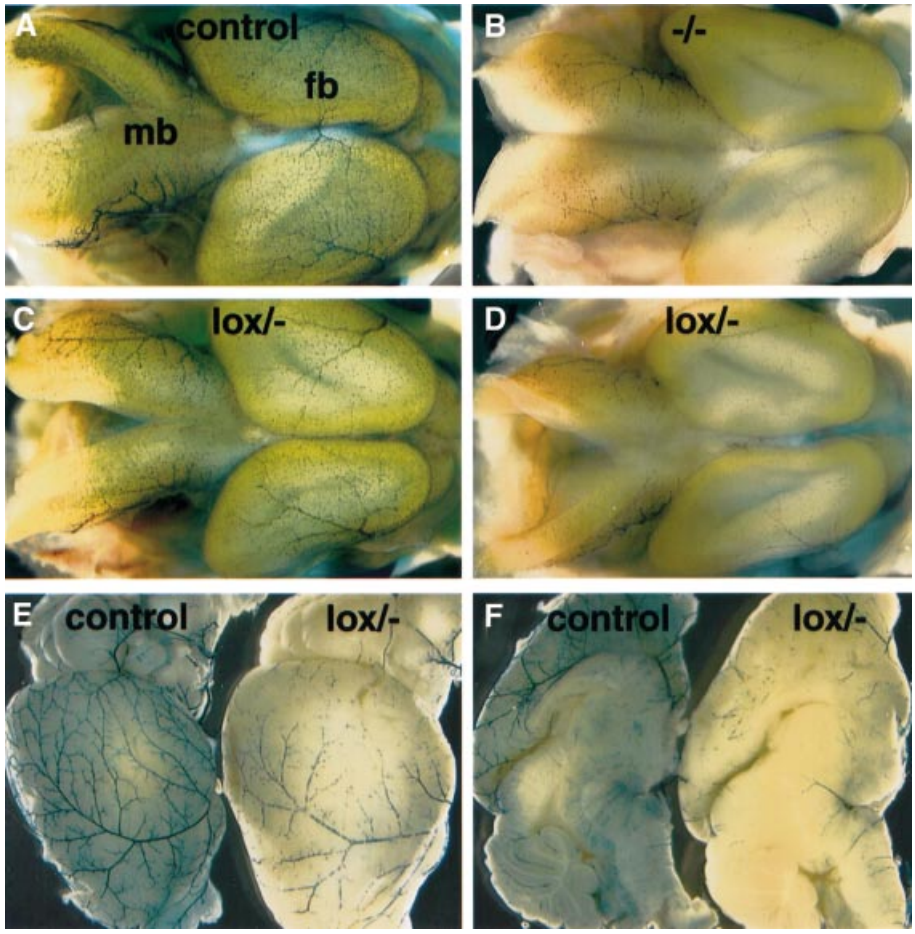

Fig. 2. Pericyte deficiency in and around the CNS in embryonic and postnatal lox/– mice. β-Gal staining of the *XlacZ4* transgene product indicates pericyte nuclei (blue). (**A**–**D**) E15.5 brains of the indicated genotypes. Two *PDGF-B*$^{lox/–}$ individuals with different degrees of pericyte loss are shown (C and D); fb, forebrain; mb, midbrain. Brains of 21-day-old control (E and F left) and lox/– (E and F right) mice viewed from the side (**E**) and from the midline (**F**).

recombinase under the control of the endothelial *Tie-1* promoter (*Tie1Cre*) (Gustafsson *et al*., 2001) with *PDGF-B*$^{+/–}$ mice, and subsequently with *PDGF-B*$^{flox/flox}$ mice. In the resulting litters, endothelium-restricted mutants (*PDGF-B*$^{lox/–}$) appeared together with different types of control analogous to *PDGF-B*$^{+/+}$ and *PDGF-B*$^{+/–}$ mice (see Materials and methods for details). In contrast to *PDGF-B*$^{–/–}$ mice, which are embryonic lethal (Levéen *et al*., 1994), *PDGF-B*$^{lox/–}$ mice were born at Mendelian ratios, reached adulthood and were fertile. To assess the efficiency of Cre-mediated recombination at the *PDGF-B* locus in capillary endothelial cells *in vivo*, we isolated capillary fragments from brains of embryonic day (E) 16.5 *PDGF-B*$^{lox/+}$ embryos, and determined the relative abundance of the flox and lox alleles by PCR (Figure 1D). There was a noticeable individual variation in flox:lox PCR fragment ratio in different individuals. Assuming equal efficiency of amplification of the wild type, flox and lox alleles, the Cre-mediated recombination of the flox allele in endothelial cells from different individuals varied between ~20 and 90% (Figure 1D).

Impaired pericyte recruitment in the CNS correlates with development of retinopathy

We bred the *Tie1Cre* transgene and the different PDGF-B alleles onto the *XlacZ4* background in order to visualize and quantify pericyte recruitment to CNS microvessels. The *XlacZ4* transgene is expressed in vSMCs and pericytes from late gestation onwards in correlation with other markers for these cells, such as α-smooth muscle actin, desmin and NG2 (Klinghoffer *et al*., 2001; Ozerdem *et al*., 2001; Tidhar *et al*., 2001; Abramsson *et al*., 2002; Stalmans *et al*., 2002). Whole-mount staining of E15.5 brains visualized the pericyte abundance and distribution in superficial CNS vessels and revealed that the pericyte density in *PDGF-B*$^{lox/–}$ embryos was intermediate between that of *PDGF-B*$^{+/+}$ and *PDGF-B*$^{–/–}$ embryos at this site. However, there was a noticeable inter-individual variation in the pericyte density between *PDGF-B*$^{lox/–}$ embryos, ranging from near normal to near complete absence (Figure 2A–D and data not shown).

The pericyte deficiency in *PDGF-B*$^{lox/–}$ mice did not normalize postnatally. The density of *XlacZ4*-positive pericytes and vSMCs was reduced in *PDGF-B*$^{lox/–}$ mutants at several sites in the CNS and in pial vessels at 3–4 weeks of age (Figures 2E and F and 3). The reduction affected arteries, veins and capillaries, which all showed intermittent stretches with very sparse coverage of *XlacZ4*-positive cells. Quantification of pericytes in four regions of the brain (pial plexus, forebrain cortex, thalamus and cerebellum) showed a similar overall degree of reduction in different regions of the same mouse, but extensive

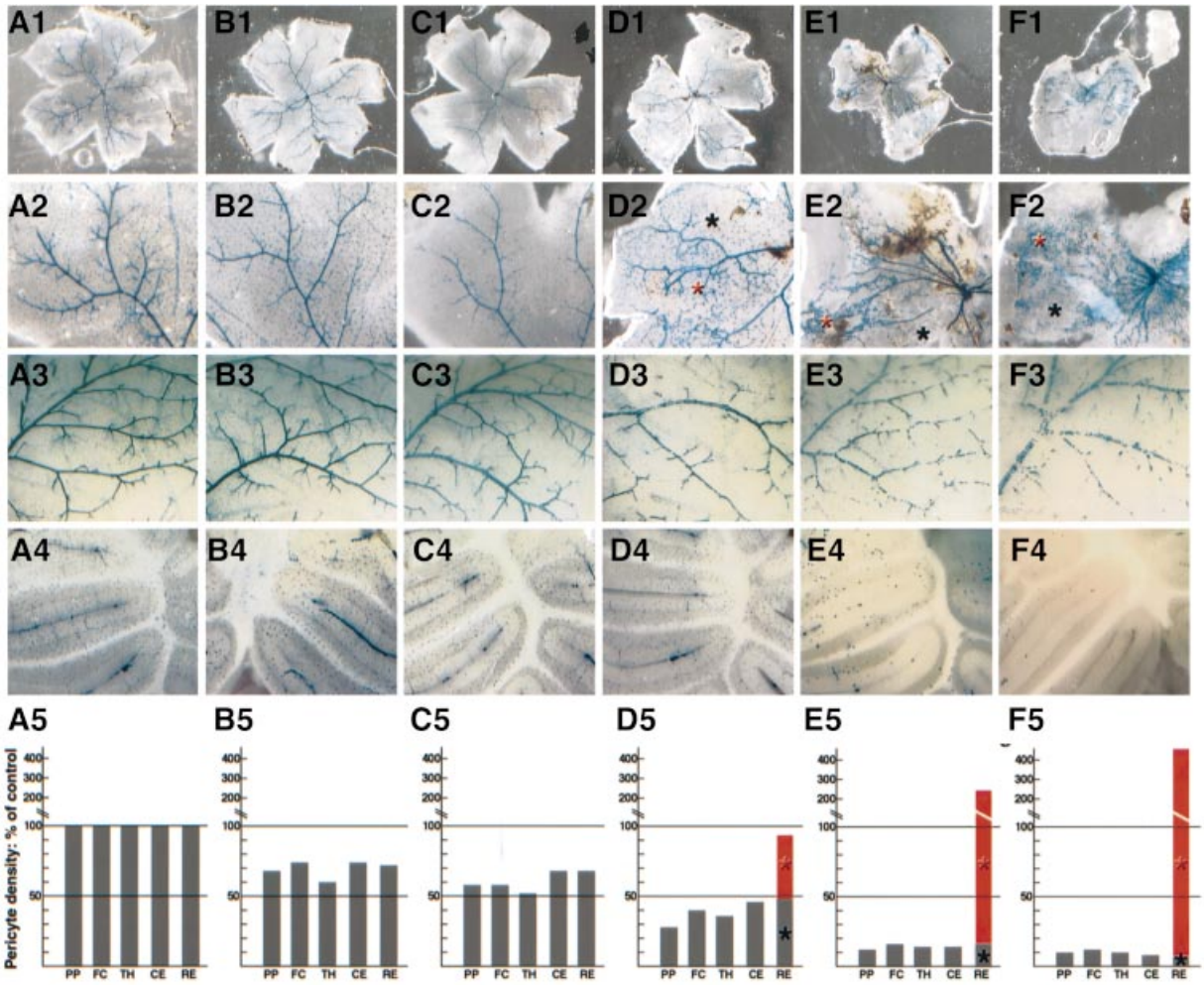

Fig. 3. Retinopathy in *PDGF-B*$^{lox/-}$ mice. The figure compares six individuals (A–F): (**A**) is wild type and (**B**–**F**) are different *PDGF-B*$^{lox/-}$ individuals) with regard to retinal status (1), pericyte density and distribution in the retina (2), pial vascular plexus (3) and cerebellum (4). Relative quantification of pericyte density at four distinct sites in and adjacent to the CNS (PP, pial plexus; FC, forebrain cortex; TH, thalamus; CE, cerebellum) is shown in A5–F5. The wild-type density for each site is set to 100%. Individuals (B) and (C), which have >50% of the normal pericyte density at other sites in the CNS, show a similar degree of pericytic coverage in the retina. Individuals (D), (E) and (F), which have <50% of the normal pericyte density at all sites investigated, show severe changes in the retina, with advanced vessel abnormalities and retinal traction. In these retinas, the density of XlacZ4-positive pericytes is highly variable (black asterisks in 2 and bars in 5 show sparse regions with similar densities to the rest of the CNS; red asterisks in 2 and bars in 5 indicate regions of increased pericyte density).

variation between individual *PDGF-B*$^{lox/-}$ mice (Figure 3). The retinas in individuals with the lowest overall CNS pericyte density, however, deviated from this correlation by displaying focal regions of increased pericyte density (Figure 3D–F, red asterisks and bars). Such retinas also showed gross abnormalities; they were contracted (Figure 3D1–F1) and often attached to the retinal pigment epithelial (RPE) cells and the lens.

At high magnification we could see distinctive vascular aberrations in all *PDGF-B*$^{lox/-}$ individuals, including variable capillary and venous diameter, irregular capillary density, abnormal capillary ring structures, increased number of regressing capillary branches and the presence of microaneurysms (Figure 4D and E and data not shown). The abundance of these types of abnormality correlated with the degree of pericyte deficiency, but in the most severely affected retinas (e.g. Figure 3D–F), they were found only in regions with low pericyte density (Figure 4B and E). In the regions with highly increased pericyte density there was a complete loss of regular vascular pattern and formation of a dense, chaotic vascular network with large numbers of endothelial cells, pericytes and possibly also other cell types (Figure 4C). We confirmed these observations by studying vascular preparations from protease-digested retinas (Figure 4F–H). These preparations also revealed in the same retinas areas of rather normal overall vascular pattern showing an increased number of acellular capillaries and pyknotic nuclei, as well as regions of chaotic vascular organization with markedly increased vascular density (Figure 4F–H).

In the regions of increased vascular density, we also saw vessel branches penetrating into the vitreous as well as from the choroid through the photoreceptor and RPE layers (Figure 5A–H). Thus, the regions with high pericyte density show the typical hallmarks of proliferative retinopathy. These regions also showed loss of organization of the neural layers and folding of the photoreceptor layer producing typical photoreceptor rosette

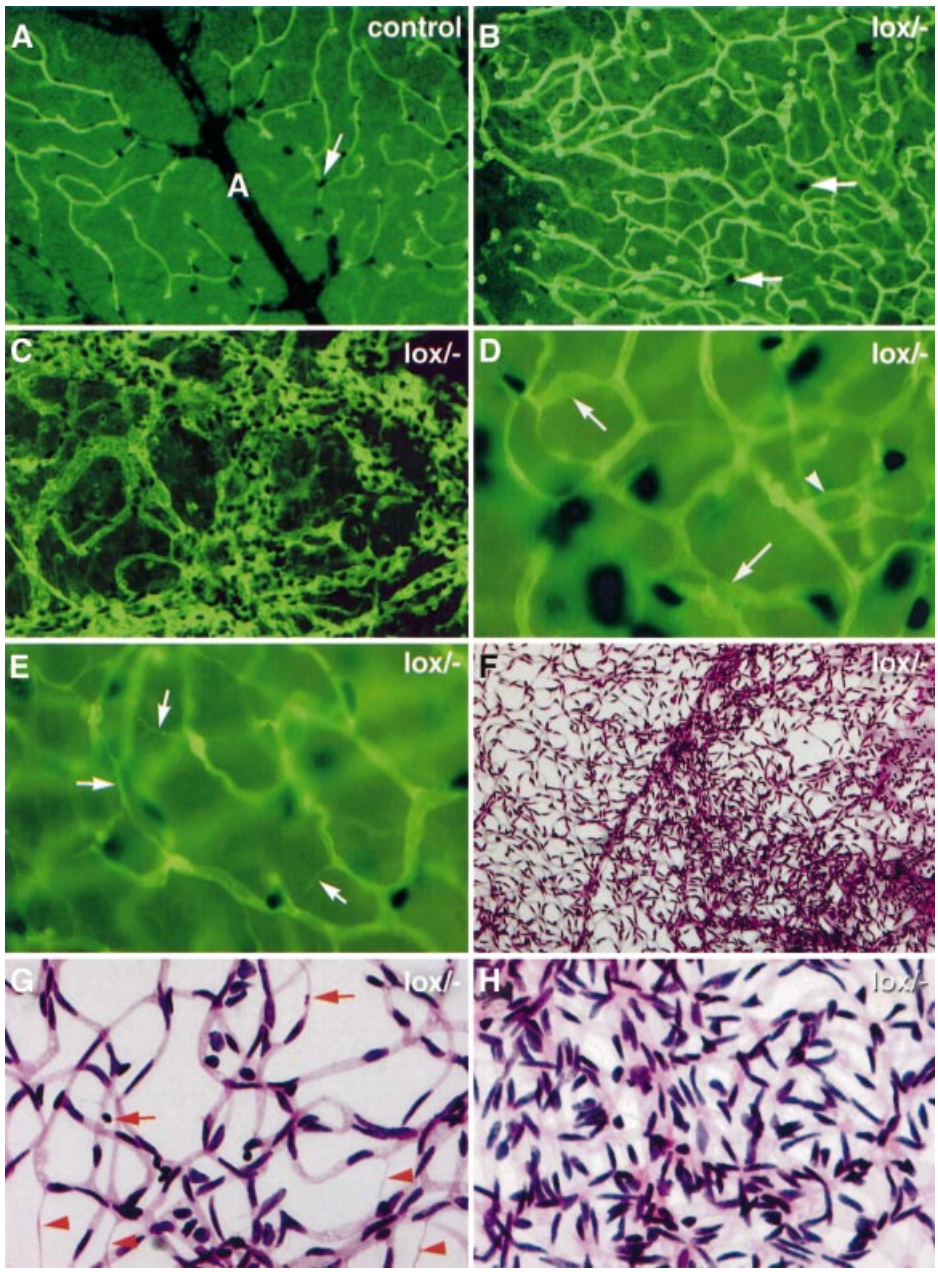

Fig. 4. Retinopathy in *PDGF-B*$^{lox/-}$ mice. Double staining of whole-mount retinas for endothelial cells (fluorescent green) and pericytes [black, e.g. white arrows in (A) and (B)]. (**A**) Part of wild-type retina in which an artery (A) with branches and associated capillary network can be seen. The *PDGF-B*$^{lox/-}$ region shown in (**B**) displays very few pericytes and a large number of tortuous and irregular vessels. The proliferative region in (**C**) shows mostly a chaotic highly proliferative vasculature with highly increased numbers of endothelial cells and pericytes. (**D**) and (**E**) show examples of the capillary network in *PDGF-B*$^{lox/-}$ individuals with >50% of the normal pericyte coverage. Note the presence of microaneurysms (arrows in D), abnormal ring structure (arrowhead in D) and regression profiles (arrows in E). (F–H) show PAS-stained protease-digested *PDGF-B*$^{lox/-}$ retinas. (**F**) shows at low magnification a region with normal vascular density (left) bordering a proliferative region (right). (**G**) shows a non-proliferative area with abundant regression profiles (red arrowheads) and pyknotic nuclei (red arrows). (**H**) shows a proliferative area at high magnification.

profiles (Figure 5A–H). Analysis of 52 mice of different genotypes showed a strong correlation between the overall CNS pericyte density and the presence of proliferative retinopathy. We chose the cerebellum as reference site for pericyte quantification in the CNS because it was easy to select analogous anatomical locations for analysis, and because cerebellum pericyte density provided a good reflection of the degree of overall CNS pericyte density (Figure 3). All individuals with <52% of the normal pericyte density in the cerebellum showed patches of proliferative retinopathy affecting at least one eye, whereas none of the individuals with >52% of the normal pericyte density showed any signs of proliferative retinopathy (Figure 5I).

Capillary regression in the outer retinal plexus correlates with proliferative retinopathy

Two interconnected vascular plexuses develop in the retina, an inner (superficial) plexus with arteries, veins and capillaries, and an outer (deep) plexus consisting mostly of

capillaries. In *PDGF-B*$^{lox/-}$ mice, both plexuses displayed characteristic abnormalities including vascular occlusion and regression. To address whether this correlated directly with pericyte deficiency, we simultaneously scored the frequency and pattern of capillary occlusion and pericyte density in the outer plexuses in a number of *PDGF-B*$^{lox/-}$

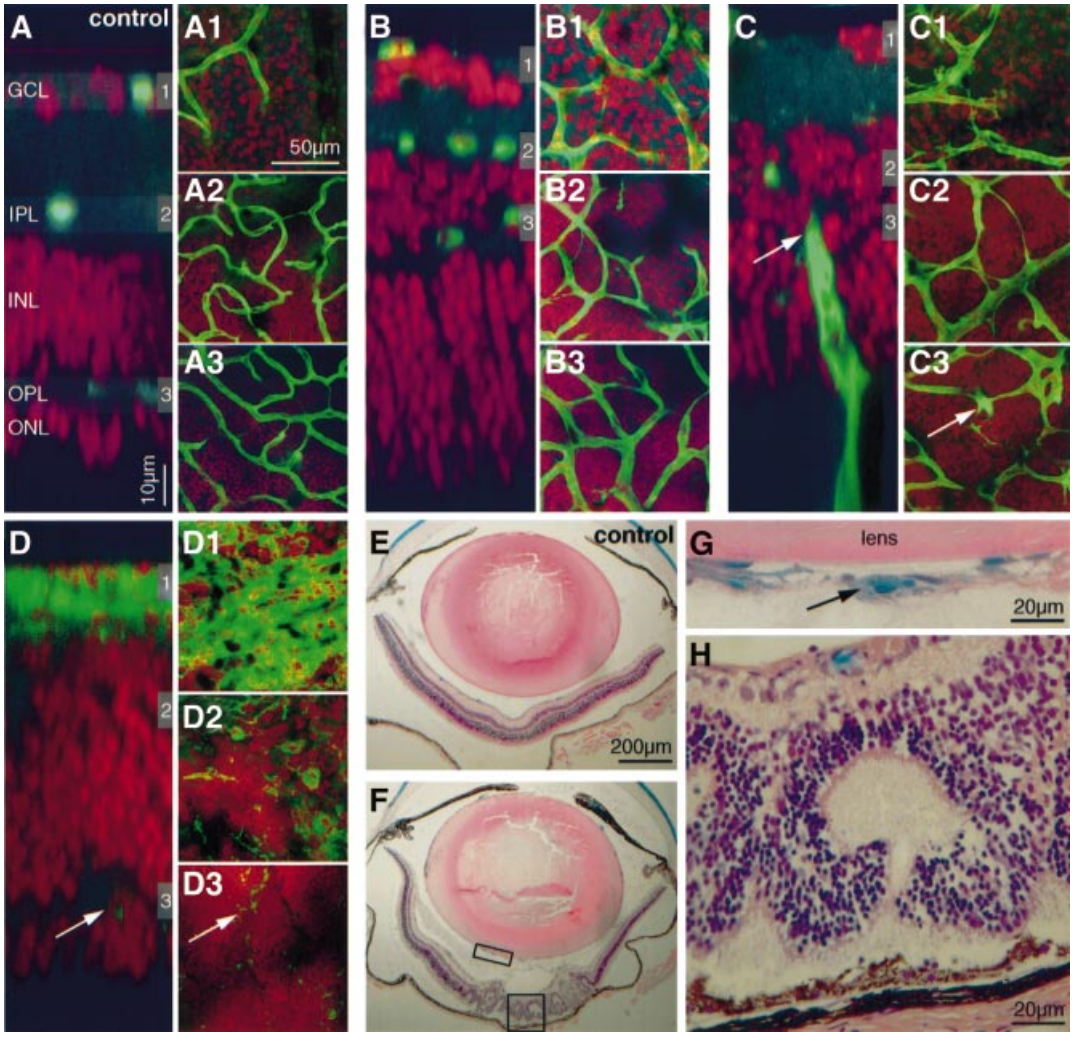

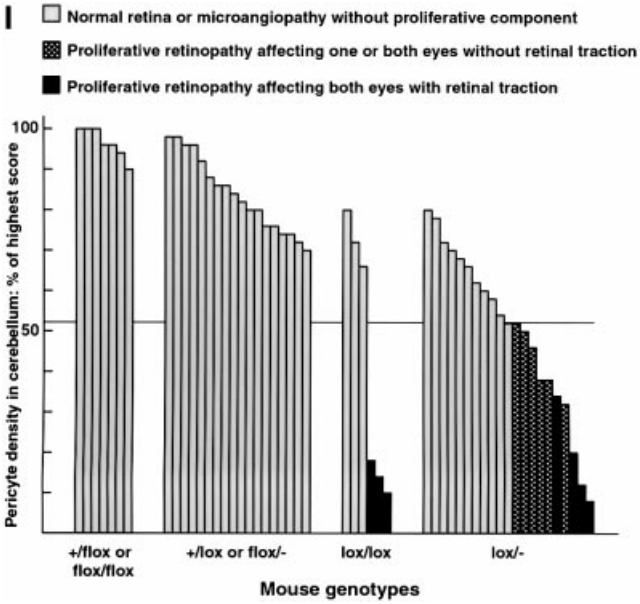

Fig. 5. Correlation between pericyte loss and retinopathy in *PDGF-B*$^{lox/-}$ mice. (**A–D**) Comparison of a control and three *PDGF-B*$^{lox/-}$ retinas affected differently by retinopathy. Double staining of vessels/microglia (fluorescent green) and nuclei (fluorescent red) of flat mounted retinas. A *z*-scan through the control retina (A) visualizes the different layers; ganglion cell layer (GCL), inner plexiform layer (IPL), inner nuclear layer (INL), outer plexiform layer (OPL) and outer nuclear layer (ONL). The gray shadowed regions numbered 1–3 indicate the levels of the corresponding pictures (A1–A3), i.e. the levels of vascular plexuses. In (B–D), note the variable thickness of the different layers, and in (C) a vessel penetrating from the choroid (arrows). In (D), the proliferative retina, total regression of the two deeper vascular plexuses leaves only scattered microglial cells in these regions (arrows). (**E** and **F**) Examples of control and *PDGF-B*$^{lox/-}$ eyes, hematoxylin and eosin staining and X-gal-positive pericytes. In (**G**), an example of pericyte-covered vessels in the vitreous is shown (magnification of rectangular box in F). Photoreceptor layer folding and disorganized neural layers leads to typical rosette formations in the severely affected retinas shown in (F) and (**H**) (magnification of squared box in F). (**I**) Fifty-two 3- to 4-week-old mice of different genotypes were scored for cerebellum pericyte density (highest set as 100%) and the presence of proliferative retinopathy. The 13 *PDGF-B*$^{lox/-}$ and *PDGF-B*$^{lox/lox}$ individuals with a pericyte density <52% all showed proliferative retinopathy affecting at least one eye.

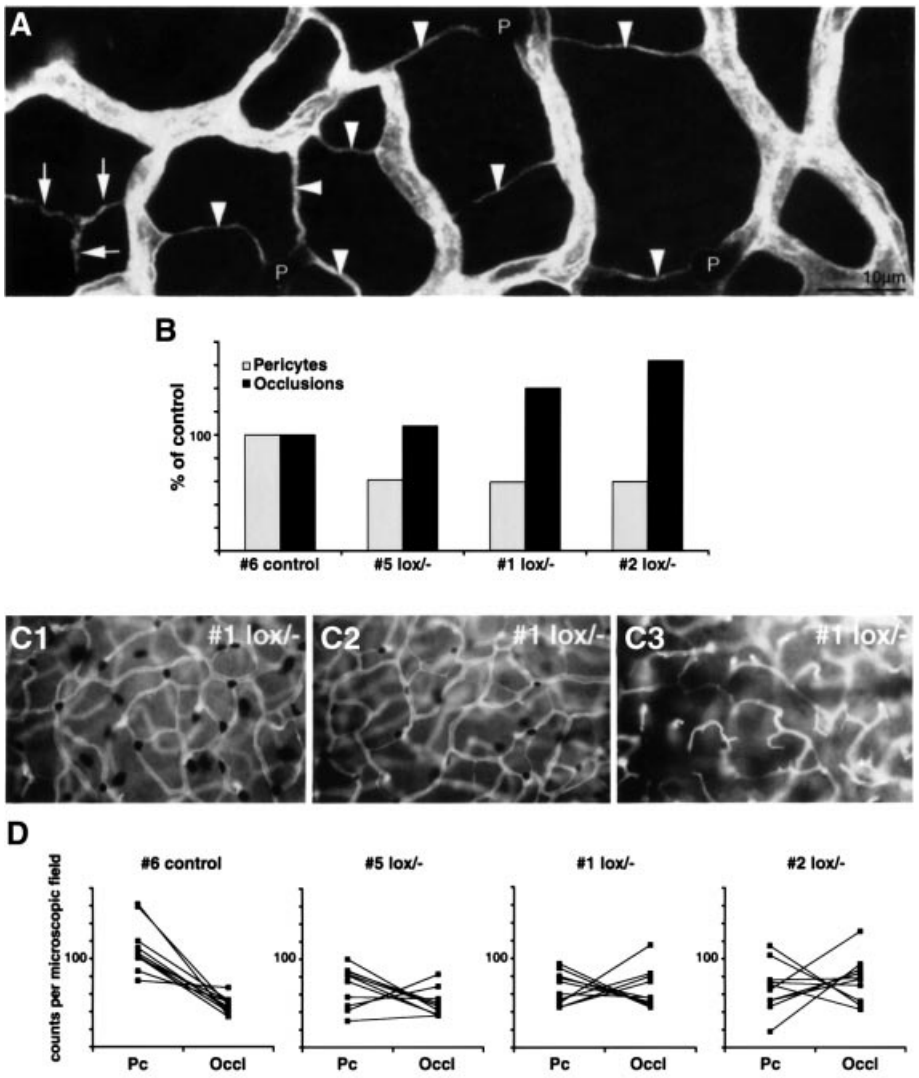

Fig. 6. Vascular regression in *PDGF-B*$^{lox/-}$ mice. Regression profiles (arrowheads in **A**) were counted in the outer retinal capillary plexus in wild type and *PDGF-B*$^{lox/-}$ with different degree of pericyte loss. (**B**) Inter-individual inverse correlation between pericyte density in the cerebellum and the density of retinal capillary regression profiles. A similar intra-individual inverse correlation is illustrated in (**C1–C3**), which show different regions of the same *PDGF-B*$^{lox/-}$ retina, ranging from near-normal pericyte density and few regression profiles (C1), and intermediate region (C2), to near-complete pericyte deficiency correlating with a high number of regression profiles (C3). A quantitative analysis further demonstrating the inverse correlation between pericyte count (Pc) and the number of occlusions (occl) is shown in (**D**). Note that the inverse correlation is seen also in controls (D, left graph), suggesting that pericyte coverage may also in part determine physiological regression. Corresponding counts from the same microscopic field are joined by a line. In *PDGF-B*$^{lox/-}$ mutant 5, an area with an almost completely regressed outer plexus showed a low number of both pericytes and occlusions.

mutants (Figure 6A). Ten random fields were analyzed in each retina, representing together about half of the retinal area. In controls, branch occlusions were observed in regular patterns. This is known to be part of the normal vessel remodeling and it affects mostly singular branches interconnecting neighboring plexus units, as defined by supplying arterioles (not shown). In contrast, *PDGF-B*$^{lox/-}$ mutants displayed both an increased density of regression profiles and a distinctive change in their pattern; several sequential branches were often affected, leading to the formation of characteristic Y-shaped, or more complex, regression profiles (Figure 6A). In addition to an inter-individual correlation between pericyte deficiency and regression (Figure 6B), there was a similar intra-individual correlation in different retinal regions, seen as an inverse correlation between number of pericytes and number of regression profiles in individual microscopic fields (Figure 6C and D). A complete lack of pericytes correlated with the complete regression of the outer plexuses (Figure 6C3). This, in turn, correlated with the occurrence of proliferative changes at the retinal surface and the formation of abnormal vascular penetration of the bottom layers of photoreceptor and RPE cells, as shown by confocal *z*-scans (Figure 5A–D).

Discussion

Previous studies have shown that pericyte progenitors express PDGFR-β and require PDGF-B for their recruitment to new vessels in the course of angiogenesis (Lindahl *et al*., 1997; Hellström *et al*., 1999; Klinghoffer *et al*., 2001). Loss of pericytes in these mutants leads to

microvascular changes similar to those typical of diabetic microangiopathy, such as the formation of microaneurysms and increased microvascular leakage. Whereas the complete knockouts of PDGF-B or PDGFR-β are lethal during late embryonic development or at birth (Levéen *et al*., 1994; Soriano, 1994), the exchange of the intracellular domain of PDGFR-β for that of PDGFR-α produced viable mice; however with a severe deficit in retinal pericytes and the development of retinopathy (Klinghoffer *et al*., 2001). These and other studies on the cardiovascular defects in PDGF-B and PDGFR-β mutant mice (Crosby *et al*., 1998; Lindahl *et al*., 1998; Ohlsson *et al*., 1999; Tallquist *et al*., 2000; Hellström *et al*., 2001), have demonstrated the critical importance of PDGF-B/PDGFR-β signaling for proper pericyte recruitment in developmental angiogenesis in a number of different organs, including the retina.

In contrast to the previous models of genetic PDGF-B or PDGFR-β deficiency, the endothelium-restricted PDGF-B knockout reported here produces a wide spectrum of pericyte-deficient states, which vary at both the inter- and intra-individual levels. This variation is most likely dependent on different degrees of chimerism with regard to PDGF-B-negative and PDGF-B-positive endothelial cells occurring as a result of variation in Cre-mediated recombination efficiency. The reason for this variation is unclear; however, genetic background is likely to play a role as we have noticed a significant degree of familial clustering of individuals with severe or mild pericyte loss and retinal changes, respectively (data not shown). Due to the crossing of mice carrying *PDGF-B* null, and flox alleles with *Tie1Cre* transgenics, the genetic background is a mixture of C57Bl6, 129 and CBA. Further inbreeding of *PDGF-B*$^{lox/-}$ mutants should allow us to determine how strong the genetic component is, and to what extent epigenetic mechanisms may also play a role, and if the variation depends on Cre-protein level, recombination efficiency at the *PDGF-B* locus, or both.

Irrespective of mechanism underlying the variation in Cre-mediated recombination and PDGF-B expression, the resulting inter- and intra-individual variation in pericyte density allowed us to analyze the effects of a wide range of pericyte-deficient states, ranging from near-normal to near-complete lack of such cells. In mutants with >50% of normal overall CNS pericyte density, the retinal vasculature displayed irregular microvessel diameter, microaneurysms and increased vascular regression. In individuals with <50% of normal pericyte density, the retinas developed regions with a massive increase of abnormal vessels extending into the vitreous and choroid. The somewhat paradoxical pericyte proliferation associated with these proliferative changes is apparently independent of endothelium-derived PDGF-B, suggesting that different mechanisms govern pericyte proliferation in association with normal or pathological angiogenesis. Importantly, regions of vascular proliferation in the inner plexus, complete outer plexus regression, and vitreous- and choroid neoangiogenesis, correlated without exception, and bordered sharply to non-proliferative regions. The inverse correlation between the numbers of pericytes and regressing capillaries at both the inter- and intra-individual levels strongly suggests that pericyte deficiency triggers capillary occlusion. This may be tolerable up to a threshold level, above which neoangiogenic responses are initiated, leading to proliferative retinopathy.

The endothelium-specific PDGF-B mutant represents a model of pericyte deficiency independent of diabetes. Since these mice develop a broad spectrum of the retinal vascular changes highly similar to the different stages of diabetic retinopathy, our data provide strong support for the view that pericyte loss constitutes an early and important causal event in the pathogenesis of diabetic retinopathy. Our data also suggest that pericyte deficiency in the retina is tolerable down to a threshold level below which proliferative retinopathy will develop. The reason why this level is not reached in response to diabetes in rodents, and consequently why diabetic retinopathy does not progress into proliferative states, remains to be established. It is possible that human and rodent pericytes are differently sensitive to hyperglycemic challenges, or alternatively, that human and rodent retinal vessels are differentially sensitive to pericyte deficiency. It is also likely that duration of the diabetic state (months in rodents compared with decades in humans) contributes to the species differences in disease progression. In humans, duration of diabetes is a major risk factor for retinopathy, and correlates with its severity (Klein *et al*., 1984a,b).

Materials and methods

Generation of PDGF-B^{flox} mice

We generated a targeting vector in which the fourth exon, which codes for the major part of the PDGF-B protein, was flanked by a loxP-flanked PGK-neo cassette in intron 3 and a single loxP fragment in intron 4 (Figure 1). We linearized the targeting vector with *Not*I and transfected and selected G418-selected E14.1 embryonic stem (ES) cells as described (Levéen *et al*., 1994). The vector had integrated by homologous recombination in approximately one-fifth of the selected clones, as judged by Southern blotting. Of ES-cell clones in which a single copy of the targeting construct had integrated correctly at the PDGF-B locus, about one-third contained the loxP site in intron 4 and two-thirds were lacking it, showing that recombination could take place on either side of this loxP site. We chose an ES-cell clone containing a single correctly integrated targeting construct (flox-neo allele) for deletion of the loxP-flanked PGK-neo cassette by transient expression of hCMV-Cre (pBS185; kindly provided by Philippe Soriano, Seattle, WA). We distinguished clones in which the PGK-neo cassette was deleted but the PDGF-B exon 4 remained (flox allele) from clones in which recombination had deleted both PGK-neo and exon 4 (lox allele) by Southern blot analysis. We created germ line chimeras and subsequently *PDGF-B*$^{flox/+}$ *PDGF-B*$^{flox/flox}$ and *PDGF-B*$^{flox/-}$ mice (Levéen *et al*., 1994). All these were born at expected Mendelian ratios, reached adulthood and were phenotypically indistinguishable from *PDGF-B*$^{+/+}$ and *PDGF-B*$^{+/-}$ mice, respectively. This and other types of analysis indicated that the *PDGF-B*^{flox} allele was functionally equivalent to the *PDGF-B* wild-type (*PDGF-B*$^{+}$) allele.

Endothelium-restricted ablation of PDGF-B

We crossed *Tie-1Cre* transgenic mice (Gustafsson *et al*., 2001) with *PDGF-B*$^{+/-}$ mice to generate *Tie1Cre*$^{+}$, *PDGF-B*$^{+/-}$ offspring, which were subsequently crossed with *PDGF-B*$^{flox/flox}$ mice to create *Tie1Cre*$^{+}$, *PDGF-B*$^{lox/-}$ (*PDGF-B*$^{lox/-}$) animals together with various controls (*Tie1Cre*$^{+}$*PDGF-B*$^{lox/+}$, *Tie1Cre*^{0}*PDGF-B*$^{flox/+}$, *Tie1Cre*^{0}*PDGF-B*$^{flox/-}$). We bred the mice onto the background of the *XlacZ4* reporter mice that express β-galactosidase in vSMCs/pericytes (Tidhar *et al*., 2001). Subsequently, we intercrossed *PDGF-B*$^{lox/-}$ mice, which generated in addition to the above-mentioned genotypes also *Tie1Cre*$^{+}$, *PDGF-B*$^{lox/lox}$ mice (*PDGF-B*$^{lox/lox}$), in which Cre must inactivate two alleles in each cell in order to generate a null situation, and *PDGF-B*$^{-/-}$ mutants (embryonic lethal). The following PCR primers were used for genotyping: BF: 5′-GGGTGGGACTTTGGTGTAGAGAAG-3′; BB1: 5′-TTTGAAGCGTGCAGAATGCC-3′; BB2: 5′-GGAACGGATTTTG-

GAGGTAGTGTC-3′; BBlox: 5′-TCTGGGTCACTGCTTCAGAATA-GC-3′.

For genotyping mice during breeding, we mixed the BF, BB1 and BB2 primers with tail or toe DNA in Gittchier buffer. Forty cycles of PCR were run as follows: 96°C 30 s, 57.9°C 30 s, 65°C 2 min. This generated diagnostic fragments of 265, 400 and 624 bp for the *PDGF-B*$^{+}$, *PDGF-B*^{flox} and *PDGF-B*$^{-}$ alleles, respectively (Figure 1C). The extent of recombination *in vivo* was controlled by PCR analysis of microvascular fragments isolated from brains of E16.5 *PDGF-B*$^{lox/+}$ embryos. The microvascular fragments were prepared essentially as described (Gargett *et al*., 2000) and contained ~80% endothelial cells, 10% pericytes and 10% non-vascular cells as judged by marker analysis. DNA isolated from the microvascular fragments was subject to a three-primer PCR using the BF, BB2 and BBlox primers (PCR and cycle program as above). This PCR protocol provides diagnostic PCR fragments of 540, 400 and 265 bp representing the *PDGF-B*^{lox}, *PDGF-B*^{flox} and *PDGF-B*$^{+}$ alleles (Figure 1C and D).

Histological analysis

We carried out whole-mount β-galactosidase staining of whole tissue and sections as described (Hogan *et al*., 1994). Pericyte densities were quantified by counting XlacZ4-positive nuclei on images captured from whole-mount preparations of various parts of the CNS (including the retina) or 300 μm thick vibratome sections studied in a dissection microscope at fixed magnification. An image area containing >300 lacZ-positive nuclei in a wild-type individual was first determined. Subsequently the same area was counted in different lox/– individuals. The number of pericytes in lox/– individuals is described as a percentage of wild type. X-gal-stained retinas were post-fixed for 10 min in 4% paraformaldehyde, followed by isolectin staining (*Bandeiraea simplicifolia*, Sigma L-2140). Retinas were incubated in 1% bovine serum albumin, 0.5% Tween in phosphate-buffered saline (PBS) overnight, washed twice in PBS pH 6.8 containing 1% Tween, 0.1 mM $CaCl_2$, 0.1 mM $MgCl_2$, 0.1 mM $MnCl_2$ (PBlec) and incubated in biotinylated isolectin (20 μg/ml in PBlec) at 4°C overnight. Following washes in PBS, isolectin was detected using 10 μg/ml of a fluorescent streptavidin conjugate (Alexa Fluor 488, Molecular Probes, S-11223). TO-PRO3 (1:1000; Molecular Probes) was used for nuclear counterstaining. Whole-mount isolectin staining on post-fixed X-gal-stained P21 brains was achieved using peroxidase-conjugated isolectin B4 from *B.simplicifolia* (Sigma L-5391). Endogenous peroxidase was blocked prior to lectin staining, by 0.6% H_2O_2 in PBS. Peroxidase activity was detected by standard DAB staining. Vibratome brain sections (200 μm) were stained with isolectin B4 as described for retinas. GFAP labeling was achieved using a polyclonal rabbit antibody (1:75, Dako Z0334) followed by Alexa-568-conjugated secondary antibody (Molecular Probes). Confocal images were taken on a Leica TCS NT microscope system and processed in Adobe Photoshop. Retinal vascular preparations were obtained using a pepsin–trypsin digestion technique as described previously (Hammes *et al*., 1991). Briefly, a combined pepsin (5% pepsin in 0.2% hydrochloric acid for 1.5 h)–trypsin (2.5% in 0.2 M Tris for 15–30 min) digestion was used to isolate the retinal vasculature. Subsequently, the samples were stained with periodic acid Schiff's (PAS) stain.

Acknowledgements

We thank Helen Hjelm and Monica Elmestam for excellent technical assistance and Per Lindahl and Mats Hellström for valuable comments on the manuscript. The study was supported by the Novo Nordisk Foundation, the Swedish Cancer Foundation, IngaBritt and Arne Lundberg Foundation, the European Community and Göteborg University. H.G. is supported by an EMBO postdoctoral fellowship.

References

Abramsson,A., Berlin,Ö., Papayan,H., Paulin,D., Shani,M. and Betsholtz,C. (2002) Analysis of mural cell recruitment to tumor vessels. *Circulation*, **105**, 112–117.

Benjamin,L.E., Hemo,I. and Keshet,E. (1998) A plasticity window for blood vessel remodelling is defined by pericyte coverage of the preformed endothelial network and is regulated by PDGF-B and VEGF. *Development*, **125**, 1591–1598.

Benjamin,L.E., Golijanin,D., Itin,A., Pode,D. and Keshet,E. (1999) Selective ablation of immature blood vessels in established human tumors follows vascular endothelial growth factor withdrawal. *J. Clin. Invest.*, **103**, 159–165.

Buscher,C., Weis,A., Wohrle,M., Bretzel,R.G., Cohen,A.M. and Federlin,K. (1989) Islet transplantation in experimental diabetes of the rat. XII. Effect on diabetic retinopathy. Morphological findings and morphometrical evaluation. *Horm. Metab. Res.*, **21**, 227–231.

Buzney,S.M., Frank,R.N., Varma,S.D., Tanishima,T. and Gabbay,K.H. (1977) Aldose reductase in retinal mural cells. *Invest. Ophthalmol. Vis. Sci.*, **16**, 392–396.

Cogan,D.G., Toussaint,D. and Kuwabara,T. (1961) Retinal vascular patterns. IV. Diabetic retinopathy. *Arch. Ophthalmol.*, **66**, 366–378.

Crosby,J.R., Seifert,R.A., Soriano,P. and Bowen-Pope,D.F. (1998) Chimaeric analysis reveals role of PDGF receptors in all muscle lineages. *Nat. Genet.*, **18**, 385–388.

Engerman,R.L. (1989) Pathogenesis of diabetic retinopathy. *Diabetes*, **38**, 1203–1206.

Gargett,C.E., Bucak,K. and Rogers,P.A. (2000) Isolation, characterization and long-term culture of human myometrial microvascular endothelial cells. *Hum. Reprod.*, **15**, 293–301.

Gustafsson,E., Brakebusch,C., Hietanen,K. and Fassler,R. (2001) Tie-1-directed expression of Cre recombinase in endothelial cells of embryoid bodies and transgenic mice. *J. Cell Sci.*, **114**, 671–676.

Hammes,H.-P., Martin,S., Federlin,K., Geisen,K. and Brownlee,M. (1991) Aminoguanidine treatment inhibits the development of experimental diabetic retinopathy. *Proc. Natl Acad. Sci. USA*, **88**, 11555–11558.

Hellström,M., Kalén,M., Lindahl,P., Abramsson,A. and Betsholtz,C. (1999) Role of PDGF-B and PDGFR-β in recruitment of vascular smooth muscle cells and pericytes during embryonic blood vessel formation in the mouse. *Development*, **126**, 3047–3055.

Hellström,M., Gerhardt,H., Kalén,M., Li,X., Eriksson,U., Wolburg,H. and Betsholtz,C. (2001) Lack of pericytes leads to endothelial hyperplasia and abnormal vascular morphogenesis. *J. Cell Biol.*, **153**, 543–553.

Hogan,B., Beddington,R., Costantini,F. and Lacy,E. (1994) *Manipulating the Mouse Embryo*: *A Laboratory Manual*. Cold Spring Harbor Laboratory Press. Cold Spring Harbor, NY.

Klein,R., Klein,B., Moss,S., Davis,M.D. and DeMets,D.L. (1984a) The Wisconsin epidemiologic study of diabetic retinopathy. II: Prevalence and risk of diabetic retinopathy when age at diagnosis is less than 30 years. *Arch. Ophthalmol.*, **105**, 520–526.

Klein,R., Klein,B., Moss,S., Davis,M.D. and DeMets,D.L. (1984b) The Wisconsin epidemiologic study of diabetic retinopathy. III: Prevalence and risk of diabetic retinopathy when age at diagnosis is 30 or more years. *Arch. Ophthalmol.*, **105**, 527–532.

Klinghoffer,R.A., Mueting-Nelsen,P.F., Faerman,A., Shani,M. and Soriano,P. (2001) The two PDGF receptors maintain conserved signaling *in vivo* despite divergent embryological functions. *Mol. Cell*, **7**, 343–354.

Levéen,P., Pekny,M., Gebre-Medhin,S., Swolin,B., Larsson,E. and Betsholtz,C. (1994) Mice deficient for PDGF B show renal, cardiovascular and hematological abnormalities. *Genes Dev.*, **8**, 1875–1887.

Li,D.Y., Sorensen,L.K., Brooke,B.S., Urness,L.D., Davis,E.C., Taylor,D.G., Boak,B.B. and Wendel,D.P. (1999) Defective angiogenesis in mice lacking endoglin. *Science*, **284**, 1534–1537.

Lindahl,P., Johansson,B.R., Levéen,P. and Betsholtz,C. (1997) Pericyte loss and microaneurysm formation in PDGF-B-deficient mice. *Science*, **277**, 242–245.

Lindahl,P., Hellstrom,M., Kalen,M., Karlsson,L., Pekny,M., Pekna,M., Soriano,P. and Betsholtz,C. (1998) Paracrine PDGF-B/PDGF-Rβ signaling controls mesangial cell development in kidney glomeruli. *Development*, **125**, 3313–3322.

Liu,Y. *et al.* (2000) Edg-1, the G protein-coupled receptor for sphingosine-1-phosphate, is essential for vascular maturation. *J. Clin. Invest.*, **106**, 951–961.

Oh,S.P., Seki,T., Goss,K.A., Imamura,T., Yi,Y., Donahoe,P.K., Li,L., Miyazono,K., ten Dijke,P., Kim,S. and Li,E. (2000) Activin receptor-like kinase 1 modulates transforming growth factor-β 1 signaling in the regulation of angiogenesis. *Proc. Natl Acad. Sci. USA*, **97**, 2626–2631.

Ohlsson,R., Falck,P., Hellstrom,M., Lindahl,P., Bostrom,H., Franklin,G., Ahrlund-Richter,L., Pollard,J., Soriano,P. and Betsholtz,C. (1999) PDGFB regulates the development of the labyrinthine layer of the mouse fetal placenta. *Dev. Biol.*, **212**, 124–136.

Ozerdem,U., Grako,K.A., Dahlin-Huppe,K., Monosov,E. and

Stallcup,W.B. (2001) NG2 proteoglycan is expressed exclusively by mural cells during vascular morphogenesis. *Dev. Dyn.*, **222**, 218–227.
Patan,S. (1998) TIE1 and TIE2 receptor tyrosine kinases inversely regulate embryonic angiogenesis by the mechanism of intussusceptive microvascular growth. *Microvasc. Res.*, **56**, 1–21.
Sims,D.E. (1986) The pericyte—A review. *Tissue Cell*, **18**, 153–174.
Soriano,P. (1994) Abnormal kidney development and hematological disorders in PDGF β-receptor mutant mice. *Genes Dev.*, **8**, 1888–1896.
Stalmans,I. *et al.* (2002) Arteriolar and venolar patterning in retinas of mice selectively expressing VEGF isoforms. *J. Clin. Invest.*, **109**, 327–336.
Suri,C., Jones,P.F., Patan,S., Bartunkova,S., Maisonpierre,P.C., Davis,S., Sato,T.N. and Yancopolous,G.D. (1996) Requisite role of angiopoietin-1, a ligand for the TIE2 receptor, during embryonic development. *Cell*, **87**, 1171–1180.
Tallquist,M.D., Klinghoffer,R.A., Heuchel,R., Meuting-Nelsen,P.F., Corrin,P.D., Heldin,C.-H., Johnson,R.J. and Soriano,P. (2000) Retention of PDGFR-β function in mice in the absence of phosphatidylinositol 3′-kinase and phospholipase C signaling pathways. *Genes Dev.*, **14**, 3179–3190.
Tidhar,A., Reichenstein,M., Cohen,D., Faerman,A., Copeland,N.G., Gilbert,D.J., Jenkins,N.A. and Shani,M. (2001) A novel transgenic marker for migrating limb muscle precursors and for vascular smooth muscle cells. *Dev. Dyn.*, **220**, 60–73.
Yang,X., Castilla,L.H., Xu,X., Li,C., Gotay,J., Weinstein,M., Liu,P.P. and Deng,C.X. (1999) Angiogenesis defects and mesenchymal apoptosis in mice lacking SMAD5. *Development*, **126**, 1571–1580.

Received May 6, 2002; revised June 13, 2002;
accepted June 19, 2002